Case Study

Neuron

Human Olfaction without Apparent Olfactory Bulbs

Highlights

- Humans can have normal olfaction without apparent olfactory bulbs
- Olfaction without apparent bulbs is seen in 0.6% of women, but not in men
- Olfaction without apparent bulbs is associated with left-handedness

Authors

Tali Weiss, Timna Soroka, Lior Gorodisky, ..., Edna Furman-Haran, Thijs Dhollander, Noam Sobel

Correspondence

tali.weiss@weizmann.ac.il (T.W.), noam.sobel@weizmann.ac.il (N.S.)

In Brief

The olfactory bulbs are the sole known relay station of odor information from nose to brain. Using MRI, Weiss et al. discover that ~4% of left-handed women have normal olfaction without apparent olfactory bulbs. How these women can smell remains unknown.

Weiss et al., 2020, Neuron *105*, 35–45
January 8, 2020
https://doi.org/10.1016/j.neuron.2019.10.006

CellPress

Neuron
Case Study

Human Olfaction without Apparent Olfactory Bulbs

Tali Weiss,[1,2,5,*] Timna Soroka,[1,2,5] Lior Gorodisky,[1,2] Sagit Shushan,[1,2] Kobi Snitz,[1,2] Reut Weissgross,[1,2] Edna Furman-Haran,[1] Thijs Dhollander,[3,4] and Noam Sobel[1,2,6,*]
[1]The Azrieli National Institute for Human Brain Imaging and Research, Weizmann Institute of Science, Rehovot, Israel
[2]Department of Neurobiology, Weizmann Institute of Science, Rehovot, Israel
[3]The Florey Institute of Neuroscience and Mental Health, Melbourne, VIC, Australia
[4]The Florey Department of Neuroscience and Mental Health, University of Melbourne, Melbourne, VIC, Australia
[5]These authors contributed equally
[6]Lead Contact
*Correspondence: tali.weiss@weizmann.ac.il (T.W.), noam.sobel@weizmann.ac.il (N.S.)
https://doi.org/10.1016/j.neuron.2019.10.006

SUMMARY

The olfactory bulbs (OBs) are the first site of odor representation in the mammalian brain, and their unique ultrastructure is considered a necessary substrate for spatiotemporal coding of smell. Given this, we were struck by the serendipitous observation at MRI of two otherwise healthy young left-handed women, yet with no apparent OBs. Standardized tests revealed normal odor awareness, detection, discrimination, identification, and representation. Functional MRI of these women's brains revealed that odorant-induced activity in piriform cortex, the primary OB target, was similar in its extent to that of intact controls. Finally, review of a public brain-MRI database with 1,113 participants (606 women) also tested for olfactory performance, uncovered olfaction without anatomically defined OBs in ~0.6% of women and ~4.25% of left-handed women. Thus, humans can perform the basic facets of olfaction without canonical OBs, implying extreme plasticity in the functional neuroanatomy of this sensory system.

INTRODUCTION

In mammalian olfaction, odorants are first transduced into neural signals at olfactory receptor neurons (ORNs) in the nose. The olfactory neural signal then travels along the axons of these neurons, through perforations in the skull (the cribriform plate), and into the brain where they target the olfactory bulbs (OBs). In rodents, this targeting is highly ordered, and this order is taken to play a critical role in odor coding (Axel, 1995; Bozza and Mombaerts, 2001; Buck, 1996; Johnson and Leon, 2007; Mori et al., 2006; Zou et al., 2009). More specifically, rodents have more than 1,000 OR subtypes, each sensitive to a subset of odorant features. The spatial ordering of these ORs in the nose is complex, but in their path to the OB they converge such that all ORNs expressing a specific receptor subtype target one of two common mirror-placed locations in the OB, termed glomeruli. Notably, this organization may follow different rules in humans, as their ~400 intact OR subtypes (Mainland et al., 2014) would predict ~800 glomeruli by this two-glomeruli-to-one-OR principle, yet postmortem studies suggest ~5,500 glomeruli and more per human OB (Maresh et al., 2008). It is widely accepted that odor coding or representation is then reflected in the spatiotemporal activity pattern across these glomeruli (Axel, 1995; Bozza and Mombaerts, 2001; Buck, 1996; Johnson and Leon, 2007; Mori et al., 2006; Zou et al., 2009). Moreover, an OB neuroanatomy that is made of intricate intra- (Luskin and Price, 1983) and inter- (Grobman et al., 2018) OB connectivity forms a highly specialized neural substrate for extended odor coding (Linster and Cleland, 2009; Schoenfeld and Cleland, 2005; Shepherd et al., 2007). Given this, one would expect that any damage to the OB should damage olfaction and that a lack of an OB altogether should result in a complete loss of the sense of smell.

There have been, however, some controversial exceptions to this rule. One study reported that, after allowing a lengthy recovery from bilateral bulbectomy, mice retained pre-bulbectomy learned olfactory aversions and could learn new olfaction-based tasks (Wright and Harding, 1982). This study, however, was criticized on a host of methodological considerations, among them a lack of histological verification for bulbectomy (Meredith et al., 1983). A second set of studies in rats implied retained olfactory capabilities after extensive OB lesions (Slotnick et al., 2004). These studies suggested that olfaction survived bulbectomy thanks to ORNs directly targeting the forebrain to form "glomeruli-like structures" in cortex (Slotnick et al., 2004), a pattern previously observed in mice (Graziadei et al., 1978). These studies as well, however, were criticized on methodological grounds, primarily suggesting that the lesions spared those aspects of the OB that were critical for the odorants tested (Leon and Johnson, 2009). These histologically based rebuttals notwithstanding, a major limitation of the studies implying retained olfaction following bulbectomy in rodents was in their reliance on performance-based measures of smell. Tasks of odorant detection and discrimination were conducted in animals that are exceptionally keen in all their sensory capabilities and, moreover, highly motivated and solely focused on the tasks at hand. This provides a lot of room for non-olfactory behavioral compensation. Such compensation may arise from any inadvertent non-olfactory information, such as the most minute auditory, visual, or somatosensory cues associated with the task.

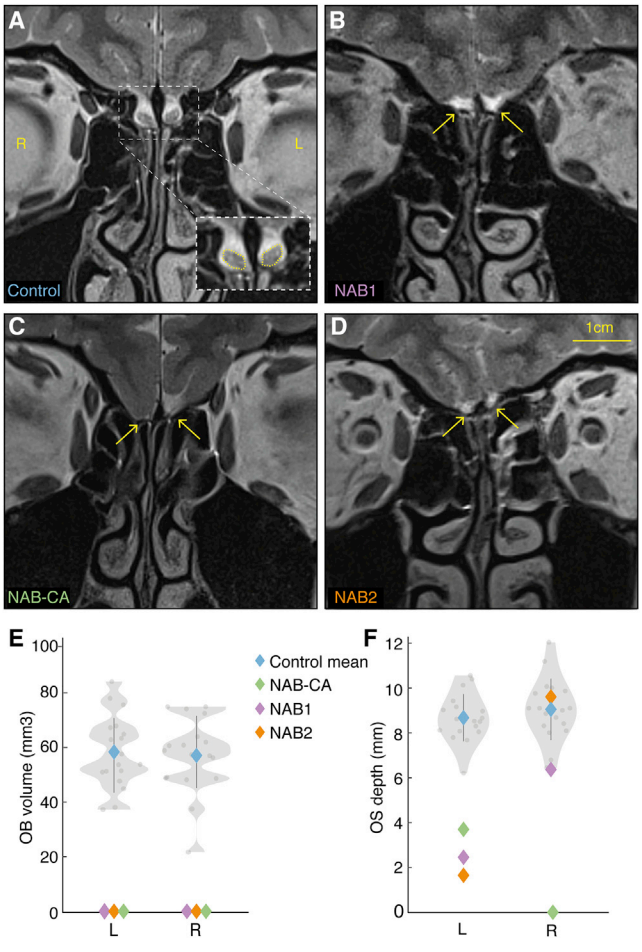

Figure 1. Structural Images of Humans without Apparent OBs

(A–D) Coronal T2-weighted MR images (cerebrospinal fluid is white) of (A) a control participant, (B) NAB1, (C) NAB-CA, and (D) NAB2. Control OBs are outlined in yellow; the area of missing OBs is marked with yellow arrows.

(E) Violin plot of OB volume measured in 36 OBs from 18 control participants.

(F) Violin plot of olfactory sulcus depth measured in 36 sulci from 18 control participants. Control participants are in gray, control mean in blue, NAB1 in purple, NAB2 in orange, and NAB-CA in green; error bar is SD. L, left; R, right. See also Figures S1–S3, S5, and S10–S12.

Moreover, even under the assumption of perfect experimental control with no non-olfactory cues, there are multiple chemosensory subsystems in the mammalian nose beyond the main olfactory system. These include the trigeminal nerve endings, the vomeronasal organ, and the Grueneberg and Septal organs, which can all transduce chemical signals (Ma, 2010). Similarly, odorants can also activate taste receptors in the mouth (Van Buskirk and Erickson, 1977). It is quite possible that some combination of activation in these subsystems enabled performance in tasks such as odorant detection and discrimination in bulbectomized rodents. In other words, bulbectomized rodents may be able to perform olfactory tasks, but the world may nevertheless smell very differently to them versus their intact conspecifics.

In turn, a measure of how the world smells is easily obtained from humans, as they can use words to convey their olfactory experience. Whereas human surgical bulbectomy typically occurs in concert with extensive additional damage to peripheral and central olfactory structures (Kim et al., 2019), an isolated lack of OBs is observed in congenital anosmia (Rombaux et al., 2009). Moreover, reductions in human OB volume may be associated with reductions in olfactory performance (Mazal et al., 2016). Given this, we were struck by the initial serendipitous observation at MRI of a woman with an intact sense of smell but without apparent OBs. In this study, we explore this observation in depth.

RESULTS

Identifying NAB1 and NAB2: Two Healthy Young Women without Apparent OBs

During MRI scanning of normosmic controls for a different study, we noticed that, in contrast to the very prominent OBs of a typical participant (Figures 1A, S1, and S2), one 29-year-old woman ("NAB1") had no apparent OBs (Figures 1B and S2; Data S1). To probe this serendipitous observation, we set out to recruit controls for two types of comparisons: the first was a 33-year-old woman with congenital anosmia ("NAB-CA"), who as expected in congenital anosmia (Rombaux et al., 2009), also has no apparent OBs (Figures 1C and S2). As a second comparison for NAB1, and particularly for functional imaging, we set out to recruit a cohort of similarly aged and similarly left-handed normosmic women with intact OBs ("bulbar controls") (Figure S1). Remarkably, at the ninth control scan, we encountered an additional participant without apparent OBs ("NAB2," age 26 years) (Figures 1D and S2; Data S2). Thus, from here on we will characterize NAB1, NAB2, and NAB-CA ("NAB group") side by side, using imaging to compare them to bulbar controls (n = 18, left-handed women age 25.9 ± 3.1 years) (Table S1), and using olfactory psychophysics to compare them to large cohorts of age-matched women.

Review of structural T2-weighted MRIs revealed that the NAB group indeed had no measurable OBs (bulbar controls OB volume: left = 58.4 ± 13.1 mm^3, right = 57.1 ± 13.6 mm^3, NAB group left and right volume was zero) (Figure 1E). The NAB group also had a significantly shallower left olfactory sulcus (bulbar control: mean = 8.68 ± 1.05 mm, NAB1 = 2.45 mm, NAB2 = 1.65 mm, NAB-CA = 3.7 mm, all two-tailed t(17) < -4.6, all $p < 0.001$, all Z-CC < −4.74) (two-tailed Crawford and Howell's modified t test, see STAR Methods) (Table S1). The right olfactory sulcus was completely absent in NAB-CA, trended toward shallower in NAB1 (bulbar control: mean = 9.05 ± 1.36 mm, NAB1 = 6.37 mm, two-tailed t(17) = −1.91, $p = 0.07$) but was typical in NAB2 (NAB2 = 9.6 mm, two-tailed t(17) = 0.41, $p = 0.7$) (Figure 1F). NAB-CA also had no apparent olfactory tracts, yet these were evident at T2 in NAB1 and NAB2. Reexamination of these findings at T1-weighted MRI revealed similar lack of OBs in the NAB group, yet poorer than T2 OB-border delineation in controls (Figure S3). Finally, we note that the NAB group had normal epithelial structures at endoscopy (see STAR Methods).

To further explore structure at microscopic scale, we acquired diffusion MRI (dMRI). Although acquired using a voxel size of 2.1 × 2.1 × 2.1 mm^3, dMRI is sensitive to anisotropic microstructure smaller than the voxel size itself (Le Bihan and Iima, 2015).

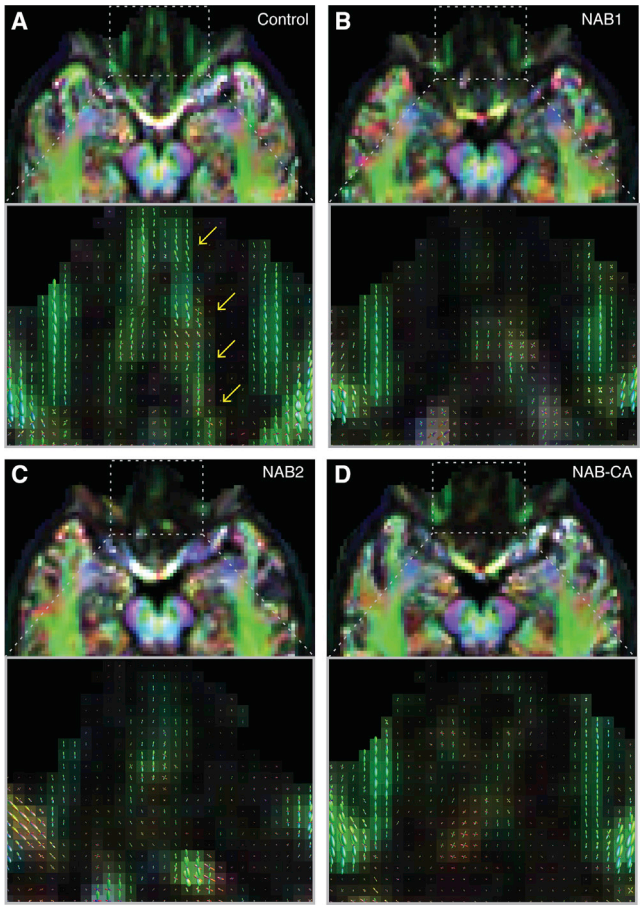

Figure 2. Diffusion-Weighed Images of Humans without Apparent OBs

(A–D) Diffusion-weighed images. Axial slices, mapped to a common template space, show FOD-based directionally encoded color (DEC) maps at the level of the olfactory tracts, for (A) control, (B) NAB1, (C) NAB2, and (D) NAB-CA. Zoomed in regions show the FODs themselves overlaid on the FOD-based DEC maps. Color code: red, left-right; green, anteroposterior; blue, superoinferior.

These data provide for white matter (WM)-like tissue fiber orientation distributions (FODs) reflecting tightly packed tracts of axons (Le Bihan and Iima, 2015). In controls, we observed clear FODs running the full length from primary olfactory (piriform) cortex to within the entire length of the OB (Figure 2A). In contrast, in NAB1 (Figure 2B) and NAB2 (Figure 2C), structure was substantially diminished, with only trace FODs, and in NAB-CA, almost all structure was lost (Figure 2D).

Finally, congenital anosmia, which is associated with no apparent OBs, is also associated with changes in brain anatomy beyond the olfactory system alone (Frasnelli et al., 2013). With this in mind, we applied whole-brain voxel-based morphometry, as well as region-of-interest-based measurements of subcortical volume and cortical thickness, yet found no brain differences in NAB1 and NAB2 beyond the olfactory system (Figure S4). The same analyses applied to NAB-CA uncovered a thicker left lateral orbitofrontal cortex in comparison to controls (control = 2.79 ± 0.11, NAB-CA = 3.05, two-tailed $t(17) = 2.32$, $p = 0.033$), yet we treat this finding with caution, as it would not survive correction for multiple comparisons had this not been a targeted region of interest (ROI). Indeed, we acknowledge that the power of this claim, namely, no additional brain differences between the NAB group and controls, is limited by the inherent limitations of comparing an individual to a group using these particular MR structural methods. Thus, minute yet significant differences may have gone unnoticed.

Although human OBs are prominent at MRI (Figure 1A; Figure S1), one may suggest that these participants may have OBs that are radically smaller than normal, and which we therefore failed to see. To estimate this, we scanned NAB2 two more times, now using an ultra-high-definition 3D imaging paradigm once at 600 × 600 × 600 μm^3 resolution, and once at 470 × 470 × 470 μm^3 resolution. At this resolution, we obtain very clear images of intact OBs in controls but still no apparent OBs in NAB2 (Figure S5; Data S3). We note that a typical human OB is ~58 mm^3 and contains ~5,500 glomeruli (Maresh et al., 2008). Thus, an OB that we would be unable to see at the resolution we used (i.e., an OB of less than one voxel) is ~0.18% of a typical OB and would contain ~10 glomeruli. Figure S5C contains depictions of what 1-voxel, 3-voxel, and 9-voxel OBs would look like and illustrates the unlikeliness of us failing to observe such structures. Thus, we conclude that in the expected location of the OBs these participants have either no OBs at all or rudimentary microscopic structures that may contain tens of glomeruli rather than the expected 5,500 glomeruli and more (more on this in the Discussion). We next continue to ask what are the olfactory capabilities of these participants with no apparent OBs.

NAB1 and NAB2 Perform Well at All the Basic Facets of Olfaction

Both NAB1 and NAB2 self-proclaimed highly acute olfaction. The subjective role of olfaction in one's life can be estimated using the standardized Subjective Importance of the Sense of Smell Questionnaire (SISSQ) (Croy et al., 2010). Given that the SISSQ is culturally variable (Seo et al., 2011), we first estimated a local norm (n = 150F, age 22–36; norm = 2.98 ± 0.37). We then observed that, unsurprisingly, NAB-CA was significantly lower than norm (NAB-CA = 1, two-tailed $t(149) = -5.33$, $p < 0.00001$, Z-CC = −5.35), yet NAB1 and NAB2 were not different from the norm (NAB1 = 3.22, two-tailed $t(149) = 0.65$, $p = 0.52$; NAB2 = 2.44, two-tailed $t(149) = -1.45$, $p = 0.15$) (Figure 3A). In other words, despite no apparent OBs, a standardized test verified a significant subjective role for olfaction in the lives on NAB1 and NAB2. We next set out to test whether this subjective sense was reflected in objective capabilities.

Two standardized tests of olfactory performance are widely applied: "Sniffin Sticks" (Hummel et al., 2007) and the University of Pennsylvania Smell Identification Test (UPSIT) (Doty et al., 1984). In Sniffin Sticks, we compared the NAB group to the age- and sex-matched norms for odorant threshold (T), discrimination (D), identification (I), and a combined score (TDI). Norm values were originally obtained from a group of ~700 women age 16–35 (Hummel et al., 2007). We observed that NAB-CA could not detect even the highest concentration of n-butanol (4%) (difference from norm: $T_{NAB-CA} = 1$, $T_{norm} = 9.39 \pm 2.56$, two-tailed

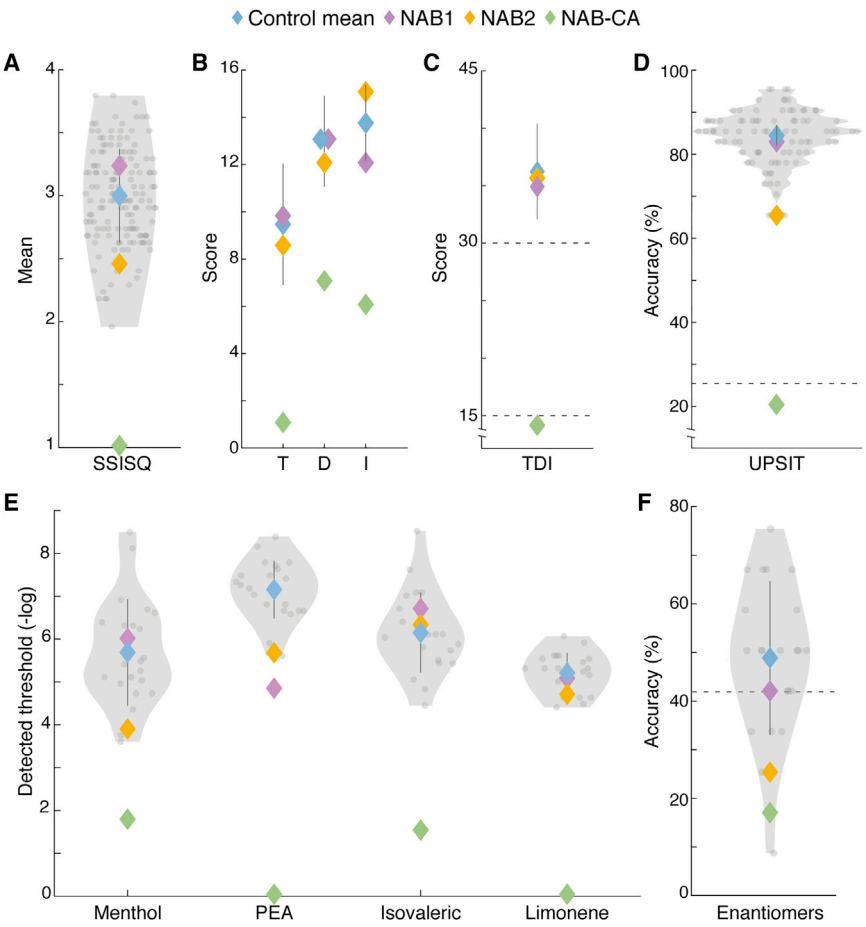

Figure 3. Intact Olfaction in Humans without Apparent OBs

In all panels: control participants in gray, control mean in blue, NAB1 in purple, NAB2 in orange, NAB-CA in green.

(A) Violin plot of Subjective Importance of the Sense of Smell Questionnaire (SISSQ) scores obtained from 150 control participants and the NAB group.

(B) Scores at olfactory threshold (T), discrimination (D), and identification (I) using the Sniffin Sticks test. Here, the normal control reflects published data from ~700 participants (hence no violin plot).

(C) Total Sniffin Sticks TDI scores. Top and bottom dashed lines reflect cutoffs for normosmia and anosmia, respectively.

(D) Violin plot of percent accuracy at University of Pennsylvania Smell Identification (UPSIT) scores obtained from 88 control participants and the NAB group.

(E) Violin plot of detection threshold scores obtained from 23 control participants and the NAB group for the odorants menthol, PEA (n = 22), isovaleric acid, and limonene.

(F)Violin plot of discrimination accuracy at the enantiomer triangle test obtained from 22 control participants and the NAB group. Dashed line is at 41.8% accuracy, reflecting d′ = 1. All error bars are SD.

See also Figure S12.

t(759) = −3.27, p = 0.001, Z-CC = −3.28) and was at chance in discrimination (D_{NAB-CA} = 7, difference from chance: p = 0.08, difference from norm: D_{norm} = 12.91 ± 1.92, two-tailed t(740) = −3.07, p = 0.003, Z-CC = −3.08) and identification (I_{NAB-CA} = 6, difference from chance: p = 0.19, I_{norm} = 13.68 ± 1.62, difference from norm: two-tailed t(826) = −4.73, p < 0.00001, Z-CC = −4.74) (Figure 3B), achieving a total TDI score of 14, which is significantly lower than the norm (TDI_{norm} = 36.06 ± 4.17, two-tailed t(703) = −5.29, p < 0.00001, Z-CC = −5.29) (Figure 3C) and is indeed considered anosmic (Hummel et al., 2007). In contrast, NAB1 registered a very low (good) detection threshold (T_{NAB1} = 9.75, difference from norm: two-tailed t(759) = 0.14, p = 0.89) and normal discrimination (D_{NAB1} = 13, difference from chance: p = 3.8 × 10^{-6}, difference from norm: two-tailed t(740) = 0.05, p = 0.96) and identification (I_{NAB1} = 12, difference from chance: p = 3.8 × 10^{-5}, difference from norm: two-tailed t(826) = −1.04, p = 0.3) (Figure 3B), combining for a totally normosmic score of TDI = 34.75 (difference from norm: two-tailed t(703) = −0.31 p = 0.75) (Figure 3C). Similarly, NAB2 registered a normal detection threshold (T_{NAB2} = 8.5, difference from norm: two-tailed t(759) = −0.35, p = 0.73), normal discrimination (D_{NAB2} = 12, difference from chance: p = 3.8 × 10^{-5}, difference from norm: two-tailed t(740) = −0.47, p = 0.64), and very high (good) identification (I_{NAB2} = 15, difference from chance: p = 1.14 × 10^{-8}, difference from norm: two-tailed t(826) = 0.81, p = 0.42) (Figure 3B), combining for a totally normosmic score of TDI = 35.5 (difference from norm: two-tailed t(703) = 0.13, p = 0.9) (Figure 3C). In other words, according to the widely validated TDI scores, NAB-CA is indeed anosmic, yet NAB1 and NAB2, despite having no apparent OBs, are completely normosmic (Figures 3B and 3C).

We next examined UPSIT results. Given that several of the 40 UPSIT odor-objects are culturally specific to the US, we first estimated a local norm (n = 88F, age 20–39; norm = 33.59 ± 2.48, i.e., 83.97% accuracy). Unsurprisingly, NAB-CA obtained a score of 20%, which is significantly worse than the norm (two-tailed t(87) = −10.3, p < 0.00001, Z-CC = −10.32) and not different from chance (chance = 25%, p = 0.82) (Figure 3D). In contrast, whereas NAB1 obtained a score of 82.5%, which is squarely within local norms (two-tailed t(87) = −0.24, p = 0.81) (Figure 3D), NAB2 obtained a lower score of 65%, which is on par with two other members of the norm cohort, still far better than chance (p = 1.1 × 10^{-7}) yet significantly lower than the norm cohort average (two-tailed t(87) = −3.05, p = 0.003, Z-CC = −3.06) (Figure 3D). However, given that using Sniffin Sticks, the very same NAB2 obtained an unusually high identification score (15 of 16 in an identical 4-alternative identification task), her lower identification score at UPSIT may reflect odorant familiarity issues. As noted, many of the UPSIT odorants are unfamiliar to non-American cohorts. The creators of the UPSIT recognized this limitation and published a short-version UPSIT consisting of a subset of 12 out of the 40 UPSIT odorants, which they labeled as culturally independent (Doty et al., 1996). We observe that NAB2 correctly scored 10 out of these 12 odorants

(chance = 3, difference from chance $p = 3.7 \times 10^{-5}$), which renders her normosmic under this UPSIT culturally independent version (Doty et al., 1996).

In addition to the above internationally standardized and validated tests, we conducted in-lab detection threshold estimations for four odorants. NAB-CA was unable to detect even the highest concentrations we used for limonene, and phenyl ethyl alcohol (PEA) but was able to detect the highest concentrations (only) of menthol (2.5%) and isovaleric acid (10%), reflecting an overwhelming difference from controls (menthol (−log10): control = 5.68 ± 1.24, NAB-CA = 1.75, two-tailed t(22) = −3.19, p = 0.004; isovaleric (−log10): control = 6.1 ± 0.91, NAB-CA = 1.5, two-tailed t(22) = −4.9, $p = 6.5 \times 10^{-5}$) (Figure 3E). NAB-CA detection of these high concentrations presumably reflects trigeminal responses (Gudziol et al., 2001). In contrast, NAB1 and NAB2 were not significantly different from controls at detecting menthol, isovaleric acid, and limonene (menthol (−log10): control = 5.68 ± 1.24, NAB1 = 5.97, two-tailed t(22) = 0.23, p = 0.82, NAB2 = 3.86, two-tailed t(22) = −1.48, p = 0.15. isovaleric (−log10): control = 6.1 ± 0.91, NAB1 = 6.67, two-tailed t(22) = 0.62, p = 0.54, NAB2 = 6.29, two-tailed t(22) = 0.22, p = 0.83. Limonene (−log10): control = 5.17 ± 0.44, NAB1 = 5.04, two-tailed t(22) = −0.28, p = 0.78, NAB2 = 4.67, two-tailed t(22) = −1.11, p = 0.27) (Figure 3E). Only for PEA, we observed that although NAB1 and NAB2 clearly detected it (detecting the 9th and 10th dilution steps, respectively, orders of magnitude above chance and above NAB-CA), they were nevertheless significantly poorer than controls (PEA (−log10): control = 7.1 ± 0.67, NAB1 = 4.8, two-tailed t(21) = −3.35, p = 0.003, Z-CC = −3.45, NAB2 = 5.64, two-tailed t(21) = −2.15, p = 0.043, Z-CC = −2.19) (Figure 3E). Finally in this series, we tested the ability to discriminate between enantiomers, namely, structural mirror images of the same molecular species (Laska and Teubner, 1999). We used a particularly difficult version of the triangle paradigm, where participants were allowed only one sniff for each of three stimuli, two containing the same enantiomer and a third containing the mirror image enantiomer, and their task is to select the odd odorant. We observed that NAB1 and NAB2 were not significantly different from the control mean (control = 48% ± 15.7%, NAB1 = 41.8%, two-tailed t(21) = −0.41, p = 0.68; NAB2 = 25%, two-tailed t(21) = −1.46, p = 0.16) (Figure 3F). The value of this final test, however, may be limited by its difficulty: chance at this task is 33% and just significant discrimination or a d-prime (d′) score of 1 is associated with 41.8% accuracy (Ennis et al., 1998). Thus, we observe that 5 of 22 bulbar participants, as well as NAB2, had d′ <1 or, in other words, could not make the discrimination. In contrast, NAB1 had a score of d′ = 1 and, along with 17 bulbar participants, could make the discrimination (Figure 3F). Taken together, the set of lab tests again implied that NAB1 and NAB2 clearly have a sense of smell, and, with the exception of reduced detection threshold for PEA, they are not significantly different from bulbar controls.

The World Smells Similarly with and without Apparent OBs

All of the above tests reflect olfactory performance-based measures. As noted in the Introduction, odorant detection and discrimination, however, may be accomplished using chemosensory subsystems beyond the olfactory system alone (Gudziol et al., 2001; Van Buskirk and Erickson, 1977; van den Heuvel and Hulshoff Pol, 2010). Hence, a potentially more important question is how does the world smell to these individuals without OBs? To address this, NAB1, NAB2, and 140 age-matched women used visual analog scales (VASs) to rate 10 odorants along each of 11 descriptors. These data can be examined in two ways: the first way is at face value, namely, the raw ratings across odorants and descriptors. We can represent each participant as a 110-value vector reflecting the 11 descriptors applied to each of the 10 odorants. For each participant, we *Z* scored this vector and calculated the Euclidean distance with all other participants. We observed that NAB1 and NAB2 do not stand out in this measure (mean Euclidean distance across participants = 12 ± 1.3, NAB1 = 13.22, two-tailed t(139) = 0.96, p = 0.33; NAB2 = 12.62, two-tailed t(139) = 0.5, p = 0.61), yet NAB-CA was significantly different (NAB-CA = 14.7, two-tailed t(139) = 2.1, p = 0.036) (Figure 4A). This similarity between NAB1, NAB2, and the group, in application of verbal descriptors to odorants, is further retained when examining each odorant and descriptor separately (Figure S6). In other words, NAB1 and NAB2 apply raw verbal descriptors to odorants as do 140 age-matched women controls. Rather than using the raw language-based representation, we can also represent each person's olfactory perception as a matrix of perceptual similarities between all odorant pairs (Secundo et al., 2015). We can precisely derive the pairwise perceptual similarity from the pairwise application of descriptors (Callegari et al., 1997). Ten odorants provide for 45 pairwise perceptual similarity values. Such a similarity matrix makes for a measure referred to as an *olfactory perceptual fingerprint* (Secundo et al., 2015), which provides for a semantics-free representation of how the world smells to an individual (Secundo et al., 2015). Such *olfactory perceptual fingerprints* remain reasonably stable over time and are linked to genetic makeup (Secundo et al., 2015). Using this approach, we can again for each participant calculate the Euclidean distance of this vector with all other participants. We again observe that NAB1 and NAB2 do not stand out in their mean distance (mean Euclidean distance across participants: 331.3 ± 77.2, NAB1 = 334.15, two-tailed t(139) = 0.037, p = 0.97; NAB2 = 353.72, two-tailed t(139) = 0.29, p = 0.77), yet NAB-CA was again significantly different (mean distance = 764.8, two-tailed t(139) = 5.6, $p = 1.15 \times 10^{-7}$) (Figure 4B). To visualize this, we used principal-component analysis (PCA) to project all participants into a space reflecting olfactory perception (Figure 4C). We observe that the perceptual fingerprints of NAB1 and NAB2 are indeed interspersed with the perceptual fingerprints of the group, yet NAB-CA stands separately (Figure 4C), but we are also impressed that NAB1 and NAB2 may be closer to each other than expected by chance. To test this impression, we measured all the pairwise distances between all participants within the PCA space. We observed that, whereas the average distance across all 9,730 pairwise comparisons provided by the 140 participants was 288.1 ± 110.4, the difference between NAB1 and NAB2 was 130.85, which is indeed closer than 96% of all comparison (p = 0.04) (Figure 4C, inlay). Taken together, these analyses imply that NAB1 and NAB2 smell the world as does an average woman of their age, yet they are more similar to each other than

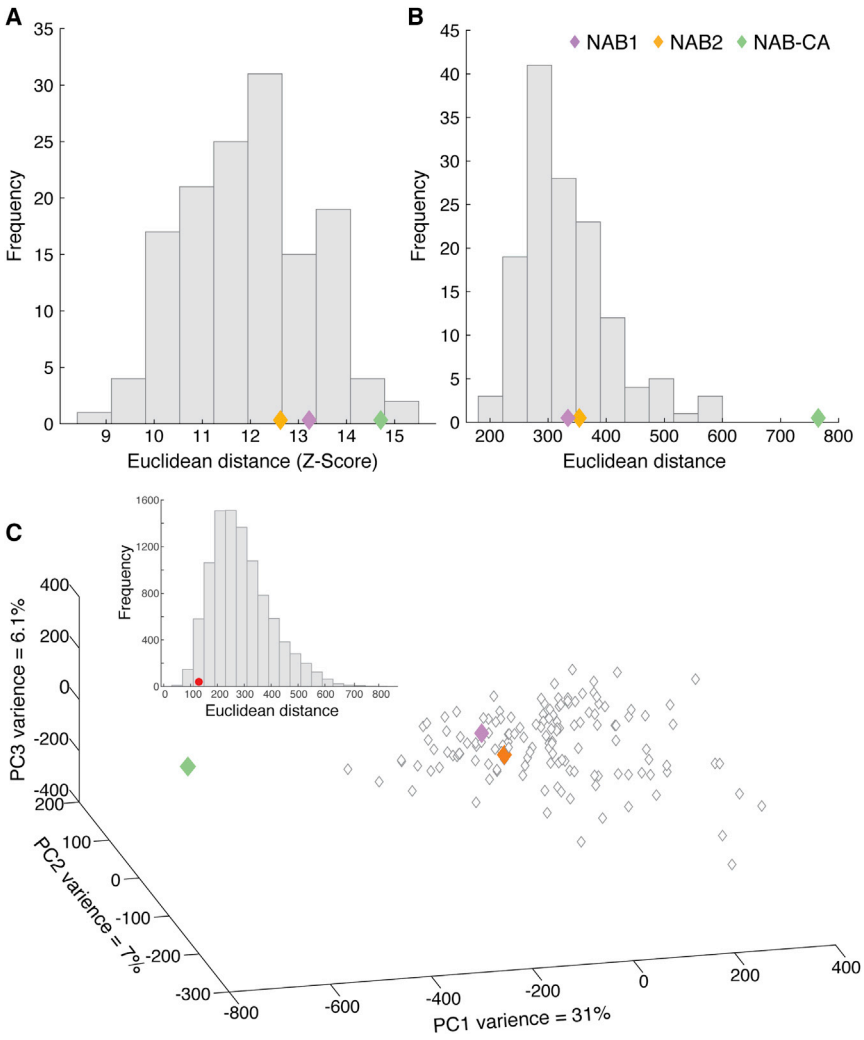

Figure 4. The World Smells Similarly with and without Apparent OBs

(A) A histogram of the distances for each participant versus all others, using the 110-value raw verbal vector.

(B) A histogram of the distances for each participant versus all others, using the 45-value pairwise odorant similarity vector.

(C) The 140 participants projected into a PCA space of olfactory perception. First 3 PCs shown. The inlay is a histogram of the pairwise distances between participants, with the distance between NAB1 and NAB2 in red. EV, explained variance. ED, Euclidean distance.

See also Figures S6 and S12.

expected by chance. Phrased differently, there may be a typical perception of the olfactory world without OBs, and this typical perception is within the range of normal perception.

Odorant-Induced fMRI Brain Activity in NAB1 and NAB2 Resembles Bulbar Controls

We next used fMRI to ask whether we see any evidence for altered odorant-induced brain activity in the NAB group (fMRI signal cannot be measured at the OB). We delivered two generally pleasant (orange and banana) and two generally unpleasant odorants (asafetida and smelly cheese) within an event-related design. In the control cohort, a group image uncovered a typical odorant-induced response, which included pronounced activation in primary (piriform) and secondary (orbitofrontal, inferior frontal gyrus, insula) olfactory regions (Figure 5A). Despite variability, a pattern of activation resembling the group image was evident in individual members of the control cohort (Figure 5B) and was similarly evident in NAB1 (Figure 5C) and NAB2 (Figure 5D). Only NAB-CA stood out in this analysis, with no odorant-induced activation at the commonly applied threshold (Figure 5E). The primary target of the OBs is piriform cortex. We therefore conducted a ROI analysis of the piriform response (Seubert et al., 2013) and observed similar odorant-induced responses in NAB1 and NAB2 versus the control group (albeit a trend toward delayed and reduced response in NAB2), and only in NAB-CA did we observe significantly less piriform activation (left piriform parameter estimate [PE]: control = 0.79 ± 0.23, NAB1 = 0.83, two-tailed $t(16) = 0.17$, $p = 0.87$, NAB2 = 0.4, two-tailed $t(16) = -1.62$, $p = 0.12$, NAB-CA = 0.11, two-tailed $t(16) = -2.86$, $p = 0.01$; right piriform PE: control = 0.85 ± 0.26, NAB1 = 1.09, two-tailed $t(16) = 0.91$, $p = 0.37$, NAB2 = 0.41, two-tailed $t(16) = -1.65$, $p = 0.12$, NAB-CA = 0.2, two-tailed $t(16) = -2.47$, $p = 0.02$) (Figures 5F and 5G). In other words, activity in the primary cortical target of the OBs was similar in NAB1, NAB2, and the bulbar control cohort, and only NAB-CA significantly differed in this respect. We conducted similar analyses in secondary orbitofrontal and insular regions. The contrast maps revealed a similar outcome of no activation in NAB-CA yet common activation patterns in NAB1, NAB2, and the control cohort (Figure S7). The data from these regions, however, were relatively noisy, such that an ROI analysis in these same structures indeed implied no differences between the group and NAB1 or NAB2 but then only a trend toward reduced activity in NAB-CA (Figure S7). We further investigated the fMRI response as a function of odorant valence (Figures S8) and conducted an investigation of functional connectivity (Figure S9). Like the signal from orbitofrontal cortex, however, these patterns were extremely variable in controls, preventing any decisive statements as to differences in NAB1 and NAB2.

About 0.6% Women and 4.25% of Left-Handed Women Have Olfaction without Apparent OBs

The identification of NAB2 while scanning controls for NAB1 raises the possibility that an apparent lack of OBs may be more common than we had thought. Moreover, that this encounter

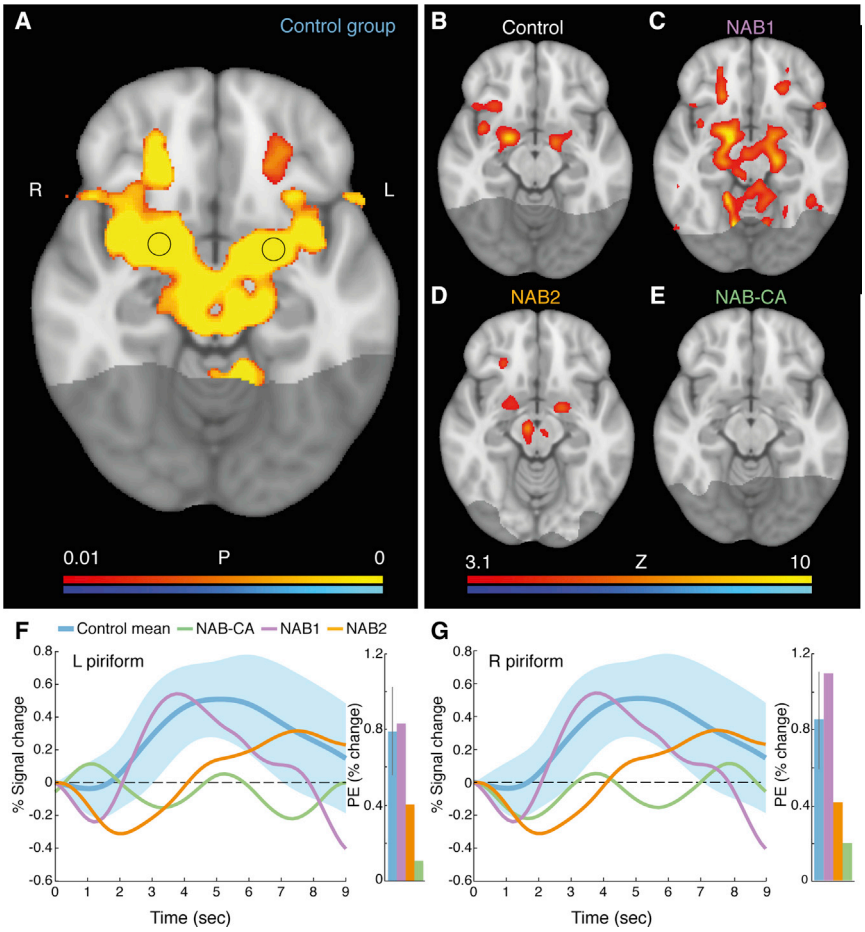

Figure 5. Typical Odorant-Induced Activity in Brains without Apparent OBs

(A) Group-image (n = 17) contrast of increased activity during odorant presence (hot colors) versus increased activity during odorant absence (cold colors), threshold free cluster enhancement (TFCE) corrected. The piriform cortex ROI is delineated. The shaded posterior section reflects the area that was not acquired in the functional scans.

(B–E) Ensuing panels reflect same contrast as in (A), but in (B) a single control participant, (C) NAB1, (D) NAB2, and (E) NAB-CA.

(F and G) Normalized percentage signal change in a ROI delineated in left (F) and right (G) piriform cortex (circle within piriform cortex in A is the ROI). Shaded area reflects SD of the mean. Inlay is a parameter estimate in percentage change values. Error bars are SD. The figure depicts positive betas only (odor > no odor). See also Figures S7–S9.

occurred while specifically scanning left-handed women further raised the possibility that such lack is somehow associated with a combination of sex and handedness. To get a sense of the possible prevalence of this phenomenon within the general population, we carefully examined the brain MRIs of 1,113 (606F, ages 22–35) participants publicly available through the Human Connectome Project (HCP) (Van Essen et al., 2013). The HCP also obtained from its participants the NIH Toolbox Odor Identification measure, a 9-item odor identification test scored and normed to have a mean = 100 ± 15. We observed 3 participants, all women (1 left handed), who had no apparent OBs (Figure 6A; Figure S10) yet, remarkably, above average olfaction scores of 110.45, 110.45, and 111.41 (age adjusted). Notably, the HCP also contained monozygotic twins of all three, and all twins had clear OBs (Figure 6B). Amusingly, we note that all three participants without apparent OBs had better olfactory scores in comparison to their intact monozygotic twins (who scored 86.45, 97.19, and 98.04, respectively) (Figure 6C). We further observed an additional participant in the HCP, again a left-handed woman, with no apparent OBs, but her MRI was relatively blurry in the ventral frontal areas, leading us to mark this participant with caution (Figure 6D; Figure S11). We note that an observation of no OBs in four women but no men in this cohort implies a strong trend toward a sex difference (two-tailed chi-square: $\chi^2 = 3.68$, $p = 0.055$). Notably, if we combine this with the results of the independent study where we serendipitously observed NAB1 (but obviously not with the continued target effort where we scanned only women), this sex difference is significant (two-tailed chi-square: $\chi^2 = 4.6$, $p = 0.032$). Moreover, we note that the HCP contains data from 47 left-handed women, thus the observation that two of four participants without bulbs were left handed implies significant association with left-handedness (two-tailed chi-square: $\chi^2 = 10.00$, $p = 0.0001$). Our local data obtained after first identifying NAB1 mirror this: once we started screening left-handed women only, out of 20 left-handed women, we encountered one normosmic woman without OBs (NAB2). Moreover, in recruiting for the normosmic bulbar control group, we encountered a hyposmic left-handed woman who, given her slightly reduced olfaction, was excluded from the intended normosmic bulbar control group. We nevertheless later independently scanned her and found that she too has no OBs (see NAB3 in Figure S12). Because unlike NAB1 and NAB2, NAB3 has slightly but significantly impaired olfaction by standardized tests (although she was unaware of this impairment), she was not systematically included in this manuscript. Nevertheless, her presentation joins a previously reported case of significantly impaired but not eradicated olfaction without apparent OBs, also in a woman (Rombaux et al., 2007). Taken together, we conclude that olfaction without apparent OBs is evident in ~0.6% of women and in ~4.25% of left-handed women.

DISCUSSION

We found that two women without apparent OBs can nevertheless perform the basic facets of olfaction. Moreover, in a large public database we found evidence for definitely three, and possibly four, additional such women. This implies that this

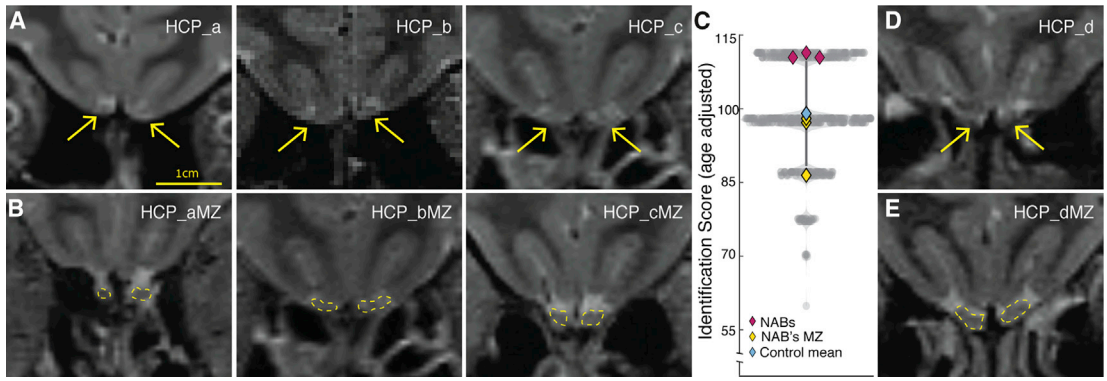

Figure 6. About 0.6% of Women and 4.25% of Left-Handed Women Have Olfaction without Apparent OBs

(A) Coronal images from three women without OBs identified in the HCP data (HCP_a-c). Yellow arrows denote expected location of OBs.

(B) Coronal images of the monozygotic twins of the three women in (A). OBs are outlined in yellow.

(C) Violin plot of olfactory performance (age-adjusted) in all 602 HCP women participants (those who have both T2 scans and olfactory tests), those without bulbs in purple, and their monozygotic twins with bulbs in yellow.

(D) Coronal image of the questionable case in the HCP data (HCP_d). Yellow arrows denote expected location of OBs.

(E) Coronal image of the mono zygotic twin of the participant in (E). OBs are outlined in yellow.

See also Figures S10 and S11.

phenomenon, although rare, was not unique to our cohort and may be evident in ~0.6% of women, and more particularly in ~4.25% of left-handed women. This result may have implications for the basic and clinical neuroscience of olfaction.

For basic neuroscience of olfaction, as noted in the introduction, there were previous reports of retained performance in olfactory tasks following bulbectomy in rodents (Slotnick et al., 2004; Wright and Harding, 1982), yet one could never be sure whether these rodents were solving the tasks with olfaction alone. Moreover, even if they were, one cannot say what bulbectomy did to their olfactory perception. In this respect, we think that the most meaningful measure in our study was not one of the measures of performance (detection, discrimination, identification) but rather the olfactory perceptual fingerprint. This measure determines how the world smells to an individual (Secundo et al., 2015). The olfactory perceptual fingerprints uncovered two findings: NAB1 and NAB2 were not significantly different from the group in how the world smells to them, but they were more similar to each other than expected by chance. This combines with the minimal reductions in performance that may have been implicated in the exacting lab tests, to imply that a lack of apparent OBs does influence olfactory perception, but it in no way prevents it.

Human olfaction without apparent OBs poses two types of questions: First, is there any facet of olfaction for which intact typical human OBs are absolutely necessary? Second, how do humans achieve the olfactory facets we observed without typical intact OBs? As to the former question, one can speculate on various facets such as olfactory learning and memory, spatial olfaction, social chemosignaling, and more, that may be more significantly impaired in these individuals, yet we did not exhaustively test. Thus, here we can only concentrate on those facets that we did test and for which intact typical OBs are apparently not absolutely necessary, namely, odorant detection, discrimination, identification, and perceptual representation. How could these facets of olfaction be achieved without apparent OBs? We see five possible explanations for our results: first, a complete intact OB may have migrated in altered development to a different brain location in the NAB participants. Although we think such a large structure would have been uncovered by the voxel-based morphometry (VBM) analysis, VBM lacks power when comparing an individual to a group, and this remains a possibility. Second, and a more likely extension of the above, is that through some process of altered development, a reshaped glomerular space sufficient to support olfaction may have formed somewhere in cortex, as implied in bulbectomized mice (Graziadei et al., 1978) and rats (Slotnick et al., 2004). This interpretation can account for our results in conjunction with current notions on olfactory coding. Third, these women may have in-place OBs that are just too tiny for us to see, even with our high-resolution scans. Although we cannot rule out this possibility, it would remain a near-equally meaningful result for the functional neuroanatomy of olfaction if humans can perform normally with OBs of ~1.6% (i.e., 9 voxels; bulbs we are very unlikely to miss, see Figure S5) the volume of typical OBs. A fourth alternative is that humans somehow use trigeminal and perhaps other chemosensory nerve endings in order to compensate for their OB loss. Although we can see how this alternative can account for task performance, if it also accounts for perceptual representation, this is truly remarkable. Finally, a fifth alternative is that coding mechanisms of human olfaction differ from those in rodents, allowing for basic olfactory facets without OBs. This is consistent with three non-rodent-like aspects in human olfactory neurobiology: (1) ratio of receptor subtypes to glomeruli (Maresh et al., 2008), (2) placement of the OB within the brain (McGann, 2017), and (3) lack of OB regeneration (Bergmann et al., 2012). Our methods could not decidedly favor any particular one of the above five interpretations, and therefore we are forced to conclude in this respect that humans can retain olfaction without apparent OBs, and we don't know how they achieve this.

As to the implications for clinical neuroscience of olfaction, congenital anosmia is associated with a lack of OBs (Rombaux et al., 2009). Given that missing OBs is probably an irreversible state, there has not been much effort directed at early detection of congenital anosmia, which, remarkably, is typically first diagnosed only in teens (Leopold et al., 1992). Indeed, why bother diagnosing anosmia early if there is nothing to be done about it? However, our observations suggest that humans can develop olfaction without apparent OBs. Assuming NAB1 and NAB2 developed olfaction through some developmental compensatory mechanisms, whether altered shaping of the olfactory system or increased capabilities of secondary chemosignaling subsystems, perhaps such compensatory mechanisms can be promoted early in life, when neural plasticity is at its highest. Currently in the West, newborns are tested for vision, audition, and more, all within the first hours or days after birth. It is perhaps time to start screening children, or perhaps even babies, using non-verbal measures of olfaction (Rozenkrantz et al., 2015). Early identification of reduced olfaction could then perhaps be addressed within an odor enrichment program (Al Aïn et al., 2019) in the aim of triggering compensatory mechanisms such as those possibly in action in NAB1 and NAB2. This could potentially prevent the many deleterious, yet widely underappreciated, outcomes associated with anosmia (Croy et al., 2014).

Our study implied that an increased incidence of olfaction without apparent OBs was associated with both female sex and left-handedness. We are puzzled by both associations. Sex is a factor in olfaction in that women typically slightly outperform men in measures of olfactory performance (Brand and Millot, 2001). Sex is also a factor in the OB ultrastructure in that women and men have similar volume OBs, but those of women contain nearly double the number of cells and neurons (Oliveira-Pinto et al., 2014). We have no hypothesis, however, as to how these sex differences might relate to the effect we observed. As to the association with left-handedness, given the link between this and altered neurodevelopment (Brandler and Paracchini, 2014), it would have been pleasing if we could probe for any functional reorganization with our fMRI measures. Olfaction fMRI, however, which is helpful for group-response representations, is just too noisy a measure for such single-subject observations (see Figure S8). Indeed, having only two participants without apparent OBs at hand can be seen as a limitation, but it in no way negates the significance of our observations. The history of neuroscience is full of important observations that were initially made in only one person. Here, olfaction in NAB1 and NAB2 has powerful implications, suggesting that humans can perform the basic facets of olfaction without apparent typical OBs, implying extreme plasticity in the functional neuroanatomy of this sensory system.

STAR★METHODS

Detailed methods are provided in the online version of this paper and include the following:

- KEY RESOURCES TABLE
- LEAD CONTACT AND MATERIALS AVAILABILITY
- EXPERIMENTAL MODEL AND SUBJECT DETAILS
  - Human Participants
- METHODS DETAILS
  - Magnetic Resonance Imaging
  - Structural Imaging Acquisition
  - Diffusion MRI Acquisition
  - Functional Imaging Acquisition
  - Odor Delivery in the MRI
  - Functional MRI Paradigm
  - Olfactory Psychophysics
  - Standardized Tests
- QUANTIFICATION AND STATISTICAL ANALYSIS
  - Structural Imaging Analysis
  - Diffusion MRI Analysis
  - Functional MRI Analysis
  - Preprocessing
  - To Generate Statistical Parametric Maps of Odorant-Induced Activation
  - To Extract Piriform Time-Course
  - To Estimate Functional Connectivity
  - To Estimate Valence-Related Activity
  - Behavioral Statistics
- DATA AND CODE AVAILABILITY

SUPPLEMENTAL INFORMATION

Supplemental Information can be found online at https://doi.org/10.1016/j.neuron.2019.10.006.

ACKNOWLEDGMENTS

This work was funded by a European Research Council AdG. grant #670798 (SocioSmell) awarded to N.S. Data were provided (in part) by the Human Connectome Project, WU-Minn Consortium (Principal Investigators: David Van Essen and Kamil Ugurbil; 1U54MH091657) funded by the 16 NIH Institutes and Centers that support the NIH Blueprint for Neuroscience Research, and by the McDonnell Center for Systems Neuroscience at Washington University. We thank Liav Tagania for initial demarcation of HCP OBs and Dr. Rita Schmidt for help in optimizing imaging parameters.

AUTHOR CONTRIBUTIONS

NAB1 Identification, T.W. and S.S.; Experimental Design, T.W., T.S., L.G., S.S., and N.S.; Experiments: T.W., T.S., L.G., S.S., and R.W.; Optimization of Scanning Parameters, E.F.-H.; Structural and Functional Data Analysis: T.W., T.S., L.G., S.S., K.S., and N.S.; Diffusion Weighted Image Analysis, T.D., Manuscript Writing, T.W., T.S., L.G., T.D., and N.S.

DECLARATION OF INTERESTS

The authors declare no competing interests.

Received: April 22, 2019
Revised: July 16, 2019
Accepted: October 1, 2019
Published: November 6, 2019; corrected online: November 15, 2019

SUPPORTING CITATIONS

The following references appear in the Supplemental Information: Gottfried and Zald (2005); Held et al. (2000).

REFERENCES

Al Aïn, S., Poupon, D., Hétu, S., Mercier, N., Steffener, J., and Frasnelli, J. (2019). Smell training improves olfactory function and alters brain structure. Neuroimage *189*, 45–54.

Andersson, J., Xu, J., Yacoub, E., Auerbach, E., Moeller, S., and Ugurbil, K. (2012). A comprehensive Gaussian process framework for correcting distortions and movements in diffusion images. In In Proceedings of the 20th Annual Meeting of ISMRM, p. 2426.

Axel, R. (1995). The molecular logic of smell. Sci. Am. *273*, 154–159.

Bergmann, O., Liebl, J., Bernard, S., Alkass, K., Yeung, M.S., Steier, P., Kutschera, W., Johnson, L., Landén, M., Druid, H., et al. (2012). The age of olfactory bulb neurons in humans. Neuron *74*, 634–639.

Bozza, T.C., and Mombaerts, P. (2001). Olfactory coding: revealing intrinsic representations of odors. Curr. Biol. *11*, R687–R690.

Brand, G., and Millot, J.L. (2001). Sex differences in human olfaction: between evidence and enigma. Q. J. Exp. Psychol. B *54*, 259–270.

Brandler, W.M., and Paracchini, S. (2014). The genetic relationship between handedness and neurodevelopmental disorders. Trends Mol. Med. *20*, 83–90.

Buck, L.B. (1996). Information coding in the vertebrate olfactory system. Annu. Rev. Neurosci. *19*, 517–544.

Callegari, P., Rouault, J., and Laffort, P. (1997). Olfactory quality: from descriptor profiles to similarities. Chem. Senses *22*, 1–8.

Crawford, J.R., and Garthwaite, P.H. (2005). Testing for suspected impairments and dissociations in single-case studies in neuropsychology: evaluation of alternatives using monte carlo simulations and revised tests for dissociations. Neuropsychology *19*, 318–331.

Crawford, J.R., Garthwaite, P.H., and Porter, S. (2010). Point and interval estimates of effect sizes for the case-controls design in neuropsychology: rationale, methods, implementations, and proposed reporting standards. Cogn. Neuropsychol. *27*, 245–260.

Croy, I., Buschhüter, D., Seo, H.-S., Negoias, S., and Hummel, T. (2010). Individual significance of olfaction: development of a questionnaire. Eur. Arch. Otorhinolaryngol. *267*, 67–71.

Croy, I., Nordin, S., and Hummel, T. (2014). Olfactory disorders and quality of life–an updated review. Chem. Senses *39*, 185–194.

Dhollander, T., and Connelly, A. (2016). A novel iterative approach to reap the benefits of multi-tissue CSD from just single-shell (+ b= 0) diffusion MRI data. 24th International Society of Magnetic Resonance in Medicine *24*, 3010.

Dhollander, T., Raffelt, D., and Connelly, A. (2017). Towards interpretation of 3-tissue constrained spherical deconvolution results in pathology. 25th International Society of Magnetic Resonance in Medicine *25*, 1815.

Doty, R.L., Shaman, P., Kimmelman, C.P., and Dann, M.S. (1984). University of Pennsylvania Smell Identification Test: a rapid quantitative olfactory function test for the clinic. Laryngoscope *94*, 176–178.

Doty, R.L., Marcus, A., and Lee, W.W. (1996). Development of the 12-item Cross-Cultural Smell Identification Test (CC-SIT). Laryngoscope *106*, 353–356.

Douaud, G., Smith, S., Jenkinson, M., Behrens, T., Johansen-Berg, H., Vickers, J., James, S., Voets, N., Watkins, K., Matthews, P.M., and James, A. (2007). Anatomically related grey and white matter abnormalities in adolescent-onset schizophrenia. Brain *130*, 2375–2386.

Ennis, J.M., Ennis, D.M., Yip, D., and O'Mahony, M. (1998). Thurstonian models for variants of the method of tetrads. Br. J. Math. Stat. Psychol. *51*, 205–215.

Fischl, B. (2012). FreeSurfer. Neuroimage *62*, 774–781.

Frasnelli, J., Fark, T., Lehmann, J., Gerber, J., and Hummel, T. (2013). Brain structure is changed in congenital anosmia. Neuroimage *83*, 1074–1080.

Friston, K.J., Buechel, C., Fink, G.R., Morris, J., Rolls, E., and Dolan, R.J. (1997). Psychophysiological and modulatory interactions in neuroimaging. Neuroimage *6*, 218–229.

Gottfried, J.A., and Zald, D.H. (2005). On the scent of human olfactory orbitofrontal cortex: meta-analysis and comparison to non-human primates. Brain Res. Brain Res. Rev. *50*, 287–304.

Graziadei, P.P., Levine, R.R., and Graziadei, G.A. (1978). Regeneration of olfactory axons and synapse formation in the forebrain after bulbectomy in neonatal mice. Proc. Natl. Acad. Sci. USA *75*, 5230–5234.

Grobman, M., Dalal, T., Lavian, H., Shmuel, R., Belelovsky, K., Xu, F., Korngreen, A., and Haddad, R. (2018). A Mirror-Symmetric Excitatory Link Coordinates Odor Maps across Olfactory Bulbs and Enables Odor Perceptual Unity. Neuron *99*, 800–813.

Gudziol, H., Schubert, M., and Hummel, T. (2001). Decreased trigeminal sensitivity in anosmia. ORL J. Otorhinolaryngol. Relat. Spec. *63*, 72–75.

Held, P., Seitz, J., Fründ, R., Nitz, W.R., Haffke, T., Hees, H., and Bonkowsky, V. (2000). MRI detection of olfactory bulb and tract. J. Neuroradiol. *27*, 112–118.

Hummel, T., Kobal, G., Gudziol, H., and Mackay-Sim, A. (2007). Normative data for the "Sniffin' Sticks" including tests of odor identification, odor discrimination, and olfactory thresholds: an upgrade based on a group of more than 3,000 subjects. Eur. Arch. Otorhinolaryngol. *264*, 237–243.

Johnson, B.A., and Leon, M. (2007). Chemotopic odorant coding in a mammalian olfactory system. J. Comp. Neurol. *503*, 1–34.

Kellner, E., Dhital, B., Kiselev, V.G., and Reisert, M. (2016). Gibbs-ringing artifact removal based on local subvoxel-shifts. Magn. Reson. Med. *76*, 1574–1581.

Kim, N., Lee, C.G., Kim, E.H., Kim, C.H., Keum, K.C., Lee, K.S., Chang, J.H., and Suh, C.O. (2019). Patterns of failures after surgical resection in olfactory neuroblastoma. J. Neurooncol. *141*, 459–466.

Laska, M., and Teubner, P. (1999). Olfactory discrimination ability of human subjects for ten pairs of enantiomers. Chem. Senses *24*, 161–170.

Le Bihan, D., and Iima, M. (2015). Diffusion magnetic resonance imaging: what water tells us about biological tissues. PLoS Biol. *13*, e1002203.

Leon, M., and Johnson, B.A. (2009). Is there a space-time continuum in olfaction? Cell. Mol. Life Sci. *66*, 2135–2150.

Leopold, D.A., Hornung, D.E., and Schwob, J.E. (1992). Congenital lack of olfactory ability. Ann. Otol. Rhinol. Laryngol. *101*, 229–236.

Linster, C., and Cleland, T.A. (2009). Glomerular microcircuits in the olfactory bulb. Neural Netw. *22*, 1169–1173.

Luskin, M.B., and Price, J.L. (1983). The topographic organization of associational fibers of the olfactory system in the rat, including centrifugal fibers to the olfactory bulb. J. Comp. Neurol. *216*, 264–291.

Ma, M. (2010). Multiple Olfactory Subsystems Convey Various Sensory Signals. In The Neurobiology of Olfaction, A. Menini, ed. (CRC Press).

Mainland, J.D., Keller, A., Li, Y.R., Zhou, T., Trimmer, C., Snyder, L.L., Moberly, A.H., Adipietro, K.A., Liu, W.L., Zhuang, H., et al. (2014). The missense of smell: functional variability in the human odorant receptor repertoire. Nat. Neurosci. *17*, 114–120.

Maresh, A., Rodriguez Gil, D., Whitman, M.C., and Greer, C.A. (2008). Principles of glomerular organization in the human olfactory bulb–implications for odor processing. PLoS ONE *3*, e2640.

Mazal, P.P., Haehner, A., and Hummel, T. (2016). Relation of the volume of the olfactory bulb to psychophysical measures of olfactory function. Eur. Arch. Otorhinolaryngol. *273*, 1–7.

McGann, J.P. (2017). Poor human olfaction is a 19th-century myth. Science *356*, eaam7263.

Meczekalski, B., Podfigurna-Stopa, A., Smolarczyk, R., Katulski, K., and Genazzani, A.R. (2013). Kallmann syndrome in women: from genes to diagnosis and treatment. Gynecol. Endocrinol. *29*, 296–300.

Meredith, M., Graziadei, P.P., Graziadei, G.A., Rashotte, M.E., and Smith, J.C. (1983). Olfactory function after bulbectomy. Science *222*, 1254–1255.

Mori, K., Takahashi, Y.K., Igarashi, K.M., and Yamaguchi, M. (2006). Maps of odorant molecular features in the Mammalian olfactory bulb. Physiol. Rev. *86*, 409–433.

Mugler, J.P., 3rd, Bao, S., Mulkern, R.V., Guttmann, C.R., Robertson, R.L., Jolesz, F.A., and Brookeman, J.R. (2000). Optimized single-slab three-dimensional spin-echo MR imaging of the brain. Radiology *216*, 891–899.

Oldfield, R.C. (1971). The assessment and analysis of handedness: the Edinburgh inventory. Neuropsychologia *9*, 97–113.

Oliveira-Pinto, A.V., Santos, R.M., Coutinho, R.A., Oliveira, L.M., Santos, G.B., Alho, A.T., Leite, R.E., Farfel, J.M., Suemoto, C.K., Grinberg, L.T., et al. (2014). Sexual dimorphism in the human olfactory bulb: females have more neurons and glial cells than males. PLoS ONE *9*, e111733.

Peres-Neto, P.R., Jackson, D.A., and Somers, K.M. (2005). How many principal components? Stopping rules for determining the number of non-trivial axes revisited. Comput. Stat. Data Anal. *49*, 974–997.

Raffelt, D., Tournier, J.-D., Fripp, J., Crozier, S., Connelly, A., and Salvado, O. (2011). Symmetric diffeomorphic registration of fibre orientation distributions. Neuroimage *56*, 1171–1180.

Rombaux, P., Mouraux, A., Bertrand, B., Duprez, T., and Hummel, T. (2007). Can we smell without an olfactory bulb? Am. J. Rhinol. *21*, 548–550.

Rombaux, P., Duprez, T., and Hummel, T. (2009). Olfactory bulb volume in the clinical assessment of olfactory dysfunction. Rhinology *47*, 3–9.

Rozenkrantz, L., Zachor, D., Heller, I., Plotkin, A., Weissbrod, A., Snitz, K., Secundo, L., and Sobel, N. (2015). A mechanistic link between olfaction and autism spectrum disorder. Curr. Biol. *25*, 1904–1910.

Schoenfeld, T.A., and Cleland, T.A. (2005). The anatomical logic of smell. Trends Neurosci. *28*, 620–627.

Secundo, L., Snitz, K., Weissler, K., Pinchover, L., Shoenfeld, Y., Loewenthal, R., Agmon-Levin, N., Frumin, I., Bar-Zvi, D., and Shushan, S. (2015). Individual olfactory perception reveals meaningful nonolfactory genetic information. Proc. Natl. Acad. Sci. USA *112*, 8750–8755.

Seo, H.-S., Guarneros, M., Hudson, R., Distel, H., Min, B.-C., Kang, J.-K., Croy, I., Vodicka, J., and Hummel, T. (2011). Attitudes toward olfaction: a cross-regional study. Chem. Senses *36*, 177–187.

Seubert, J., Freiherr, J., Djordjevic, J., and Lundström, J.N. (2013). Statistical localization of human olfactory cortex. Neuroimage *66*, 333–342.

Shepherd, G.M., Chen, W.R., Willhite, D., Migliore, M., and Greer, C.A. (2007). The olfactory granule cell: from classical enigma to central role in olfactory processing. Brain Res. Brain Res. Rev. *55*, 373–382.

Siegel, J.S., Power, J.D., Dubis, J.W., Vogel, A.C., Church, J.A., Schlaggar, B.L., and Petersen, S.E. (2014). Statistical improvements in functional magnetic resonance imaging analyses produced by censoring high-motion data points. Hum. Brain Mapp. *35*, 1981–1996.

Slotnick, B., Cockerham, R., and Pickett, E. (2004). Olfaction in olfactory bulbectomized rats. J. Neurosci. *24*, 9195–9200.

Snitz, K., Perl, O., Honigstein, D., Secundo, L., Ravia, A., Yablonka, A., Endevelt-Shapira, Y., and Sobel, N. (2019). SmellSpace: An Odor-Based Social Network as a Platform for Collecting Olfactory Perceptual Data. Chem. Senses *44*, 267–278.

Sobel, N., Prabhakaran, V., Desmond, J.E., Glover, G.H., Sullivan, E.V., and Gabrieli, J.D. (1997). A method for functional magnetic resonance imaging of olfaction. J. Neurosci. Methods *78*, 115–123.

Soler, Z.M., Hyer, J.M., Karnezis, T.T., and Schlosser, R.J. (2016). The Olfactory Cleft Endoscopy Scale correlates with olfactory metrics in patients with chronic rhinosinusitis. Int. Forum Allergy Rhinol. *6*, 293–298.

Tournier, J.-D., Smith, R., Raffelt, D., Tabbara, R., Dhollander, T., Pietsch, M., Christiaens, D., Jeurissen, B., Yeh, C.-H., and Connelly, A. (2019). MRtrix3: A fast, flexible and open software framework for medical image processing and visualisation. NeuroImage *202*, 116137.

Tustison, N.J., Avants, B.B., Cook, P.A., Zheng, Y., Egan, A., Yushkevich, P.A., and Gee, J.C. (2010). N4ITK: improved N3 bias correction. IEEE Trans. Med. Imaging *29*, 1310–1320.

Van Buskirk, R.L., and Erickson, R.P. (1977). Odorant responses in taste neurons of the rat NTS. Brain Res. *135*, 287–303.

van den Heuvel, M.P., and Hulshoff Pol, H.E. (2010). Exploring the brain network: a review on resting-state fMRI functional connectivity. Eur. Neuropsychopharmacol. *20*, 519–534.

Van Essen, D.C., Smith, S.M., Barch, D.M., Behrens, T.E., Yacoub, E., and Ugurbil, K.; WU-Minn HCP Consortium (2013). The WU-Minn human connectome project: an overview. Neuroimage *80*, 62–79.

Veraart, J., Fieremans, E., and Novikov, D.S. (2016). Diffusion MRI noise mapping using random matrix theory. Magn. Reson. Med. *76*, 1582–1593.

Woolrich, M.W., Ripley, B.D., Brady, M., and Smith, S.M. (2001). Temporal autocorrelation in univariate linear modeling of FMRI data. Neuroimage *14*, 1370–1386.

Wright, J.W., and Harding, J.W. (1982). Recovery of olfactory function after bilateral bulbectomy. Science *216*, 322–324.

Yushkevich, P. (2006). ITK-SNaP integration, NLM insight, http://www/itk org/index.htm [Accessed July 27, 2005].

Zou, D.-J., Chesler, A., and Firestein, S. (2009). How the olfactory bulb got its glomeruli: a just so story? Nat. Rev. Neurosci. *10*, 611–618.

STAR★METHODS

KEY RESOURCES TABLE

REAGENT or RESOURCE	SOURCE	IDENTIFIER
Deposited Data		
Raw and processed MRI data	This paper	https://openneuro.org/datasets/ds002185
Software and Algorithms		
MATLAB R2018a	Mathworks	https://www.mathworks.com/
Freesurfer version 6.0	Fischl, 2012	http://surfer.nmr.mgh.harvard.edu/
FSL	FMRIB, Oxford	https://fsl.fmrib.ox.ac.uk/fsl/fslwiki/
ITK-SNAP version 3	Yushkevich, 2006	http://www.itksnap.org/pmwiki/pmwiki.php
MRtrix3	Tournier et al., 2019	https://www.mrtrix.org/
MRtrix3Tissue		https://3Tissue.github.io/
Olfactory bulb demarcation software	This paper	https://gitlab.com/liorg/OlfactoryBulbDelineation

LEAD CONTACT AND MATERIALS AVAILABILITY

Further information and requests for resources and reagents should be directed to and will be fulfilled by the Lead Contact, Noam Sobel (noam.sobel@weizmann.ac.il).

EXPERIMENTAL MODEL AND SUBJECT DETAILS

Human Participants

In addition to the NAB group (n = 4) and the bulbar control group (n = 18, age 25.9 ± 3.1) who participated in both imaging and behavioral experiments (PEA threshold and enantiomer discrimination), 4 additional subjects were added for the those two test (n = 21, age 26.7 ± 3.3), 23 additional women (age 25.7 ± 3.8) participated in threshold testing (Menthol, Limonene, Isovaleric), 150 women (age 29.1 ± 3.9) participated in the SSISQ experiment, 88 women (age 30.3 ± 5.5) participated in the UPSIT experiment, and 140 women (age 27.3 ± 4.6) participated in the olfactory perceptual space experiment. For the bulbar control group, left-handedness was verified using the Edinburgh Handedness Inventory (Oldfield, 1971). All subjects reported to be with no history of significant medical illness, psychiatric disorder, or olfactory dysfunction. All participants provided written informed consent to procedures consistent with the declaration of Helsinki, and that were approved by the Weizmann Institute IRB committee.

The NAB group underwent extensive medical interview by physician to rule out any related hormonal imbalances or syndromes associated with OB atrophy (Meczekalski et al., 2013). We further ruled out any history of brain trauma, acute infection of the upper respiratory airway, sinonasal or brain disease, drug or toxic exposure. Finally, anatomical imaging and endoscopic examination revealed only minor septal deviation, and ruled out any significant peripheral abnormalities or obstructions, such that all three scored a perfect 0/10 at the olfactory cleft endoscopy scale (OCES) (Soler et al., 2016).

METHODS DETAILS

Magnetic Resonance Imaging

MRI was performed using a 3-Tesla scanner (Siemens MAGNETOM Prisma) and a 32-channel receive head-neck coil (Siemens, Erlangen, Germany).

Structural Imaging Acquisition

For OB volume and olfactory sulcus depth, images were acquired using a T2-weighted TSE sequence in the coronal plane, covering the anterior and middle segments. Sequence parameters: 30 slices, voxel size: 400 × 400 μm, slice thickness: 1.6 mm, no gap, TE = 85 ms, TR = 5000 ms, flip angle = 120°. For higher resolution images we used a 3D T2-weighted SPACE (sampling perfection with application-optimized contrasts using different flip angle evolutions) sequence (Mugler et al., 2000): TE = 94 ms, TR = 2000 ms, flip angle = 120°, bandwidth = 135 Hz/pixel, turbo factor = 80. We applied this sequence once using FOV of 200 × 200 mm^2 to achieve isotropic voxels of 600 × 600 × 600 μm^3, and once using FOV of 150 × 150 mm^2, to achieve isotropic voxels of 470 × 470 × 470 μm^3. These images were acquired in the axial plane and reformatted to sagittal and coronal planes.

Diffusion MRI Acquisition

We used a monopolar spin-echo echo-planar imaging (SE-EPI) diffusion weighted sequence acquired in the axial orientation: TR = 6500 ms, TE = 62 ms, BW = 1852 Hz/pixel, echo spacing = 0.62 ms, FOV = 210 × 210 mm^2, matrix = 100 × 100 mm^2, voxel size of 2.1 × 2.1 × 2.1 mm^3. We acquired three unweighted (b = 0) volumes, and 64 homogeneously distributed gradient directions (b-value = 1200 s/mm^2) covering a half sphere, using iPAT = 2.

Functional Imaging Acquisition

For optimal EPI acquisition quality of the primary olfactory areas, the FOV was limited to the ventral aspects of the brain. We used a T2*-weighted gradient-echo EPI sequence with the following parameters: TR = 1500 ms, TE = 25 ms, flip angle = 70°, FOV = 220 × 220 mm^2, matrix = 110 × 110 mm^2, 2 × 2 × 2 mm^3 isotropic voxels, no gap, 27 slices, GRAPPA-2 acceleration. Image acquisition was tilted at 15° off AC/PC plane to reduce susceptibility artifact in olfactory regions. An anatomical image substrate was acquired using a 3D T1-weighted MP-RAGE (magnetization prepared rapid gradient echo) sequence, with the following parameters: TR = 2300 ms, TE = 2.32 ms, TI = 900 ms, flip angle = 8°, FOV = 256 × 256 mm^2, 192 slices, resolution 0.94 × 0.94 mm^2, slice thickness: 0.9 mm, GRAPPA-2 acceleration.

Odor Delivery in the MRI

We used a computer-controlled olfactometer similar to those previously described in detail (Sobel et al., 1997) with one modification: rather than a nasal mask, we converted the entire head-coil into a controlled olfactory microenvironment. The head-coil was first enclosed with clear Teflon-coated Plexiglas. The olfactometer Teflon nosel was placed ~10 cm anterior to the nose, and a powerful 2-inch vacuum hose was connected to the back of the head coil. This generated a constant flow of air through the head-coil, and the added constant flow of olfactometer air (1.5 LPM) carried embedded pulses of odorant. This arrangement freed the participant of the cumbersome mask, and made for a natural changing odor environment. Nasal airflow was constantly precisely monitored by spirometer (ML141, ADInstruments), and instrumentation amplifier (Power-Lab 16SP, ADInstruments), allowing for odorant-triggering by respiratory trace.

Functional MRI Paradigm

Four odorants with previously-verified iso-intense perception were used: Banana oil, Orange oil (these two from Frutarom Inc. Israel), Asafetida oil (from DreamAir, NYC, USA), and smelly cheese (isovaleric acid CAS no. 503-74-2, from Sigma-Aldrich, Israel). In each of two functional runs, we delivered 10 stimuli per valence, culminating in 20 pleasant and 20 unpleasant odorant events in both runs. Stimulus duration = 3 s, inter-stimulus-interval = 20-26 s (jittered), odorant onset triggered by inhalation onset. Participants were instructed to breathe naturally, to keep their eyes closed, and if they noted an odorant, to rate odorant pleasantness (1 to 4) using a button box placed in their dominant (left) hand.

Olfactory Psychophysics

All testing was conducted in rooms specially designed for olfactory psychophysics. The rooms are coated in stainless steel, and subserved by high flow HEPA and Carbon filtration, so as to prevent odorant contamination across trials and participants.

Standardized Tests

We used two standardized tests: "Sniffin' Sticks" (Hummel et al., 2007) and University of Pennsylvania Smell Identification Test (UPSIT) (Doty et al., 1984).

Sniffin Sticks (Hummel et al., 2007) uses pen-like odor dispensing devices. It comprises three tests of olfactory function: **1. n-butanol detection threshold** using a single-staircase, 3-alternative forced choice (3AFC) procedure. There are 16 dilutions in a geometric series starting from a 4% n-butanol solution. Three pens were presented in randomized order, with two containing the solvent and the third containing the odorant. Subjects had to identify the odorant-containing pen. Reversal of the staircase was triggered when the odor was correctly identified in two successive trials. Threshold was defined as the mean of the last four of seven staircase reversals. Scores range between 1 and 16. **2. Odor discrimination** between 16 pairs of odorants, again using a 3-AFC procedure. Scores range from 0 to 16. **3. Odor identification** for 16 common odorants, using a 4-alternative forced choice procedure. Scores range between 0 and 16. A composite "TDI score" reflects the sum of the results obtained for threshold, discrimination, and identification.

The UPSIT (Doty et al., 1984) consists of 4 booklets, each containing 10 scratch-and-sniff odorants, one odorant per page (40 total). The odorants are embedded in a patch of microencapsulated crystals located on each page. Above each odorant there is a multiple-choice question with four alternative responses for each item. After scratching and smelling the odorant for as long as they want, participants were asked to select one of the four alternatives even if no smell was perceived. The participant's score was determined as the percent correct identification.

Lab-based olfaction tests: To determine detection threshold, we used a triple-forced-choice ascending staircase paradigm with 7 reversals. A geometric series of odorant dilutions were prepared for four odorants: Phenyl ethyl alcohol (PEA, CAS no. 60-12-8, a rose-like odor) and Limonene (CAS no. 5989-27-5, an orange-like odor) were diluted in mineral oil (Sigma-Aldrich), Menthol (CAS no. 15356-60-2, 26mg/ml) and 10% Isovaleric acid (CAS no. 503-74-2, a cheese-like odor) were diluted in 1,2 propandiol. On

each trial, a participant was presented with three opaque jars, one containing an odorant dilution, and two containing solvent alone. The participant was asked to sniff each jar, and indicate which jar contained the odorant. There was a 40 s ISI. An experiment started at a seven log concentration step for PEA and limonene and nine log concentration step for menthol and isovaleric. If the participant was incorrect, the next trial contained the next higher concentration. This increase in concentration continued until a point of three consecutive correct detections of a given concentration, after which the following trial shifted to a lower concentration (reversal). Whereas incorrect detection then led to concentration re-increase (reversal), two additional consecutive correct detections led to an additional concentration decrease. The average of the last four staircase reversal points out of a total of seven reversals was used as the threshold estimate.

To test enantiomer discrimination, we used a three-alternative forced choice discrimination task for two types of enantiomers: (1S)-(−)-α-Pinene (CAS no. 80-56-8) versus (1R)-(+)-α-Pinene (CAS no. 7785-70-8) and L-carvone (CAS no 6485-40-1) versus D-Carvone (CAS no 2244-16-8) all undiluted, 0.05 mL in each jar. In each of 12 trials (6 of each type) three opaque jars were presented to the participant in a randomized order. Participants were allowed to take only one sniff at each odor presentation (with no repetition), and were then asked to pick out the jar that contained the dissimilar odor.

To determine an olfactory perceptual fingerprint (Secundo et al., 2015), we used SmellSpace (Snitz et al., 2019). Participants used online visual-analog scales (VAS) to rate each of 10 scratch-and-sniff odorants (SmellSpace II: Rose, Cumin, banana, Asafetida, Maple, Strawberries, Violet, Eucalyptus, Guava, and Anis, all provided by DreamAir, NYC, USA) along each of 11 verbal descriptors (VASs ranging from "not at all" to "very": Pleasant, Intense, Bitter, Chemical, Spicy, Sweet, Burnt, Fruity, and Garlic; VASs ranging between two descriptors: Fresh-Rotten, Clean-Dirty). To compare olfactory perception across participants, we used two different approaches, one language-dependent, and the other semantics-free. For language-dependent comparisons, for each participant we generated a 110-value vector made of the 11 descriptor values applied to each of the 10 odorants. This vector was Z-scored for comparisons across participants. For semantics-free comparison we generated for each participant an olfactory perceptual fingerprint (Secundo et al., 2015), namely a similarity matrix reflecting all the derived pairwise similarity ratings using the 10 odorants, i.e., 45 pairwise similarity ratings. We then calculated Euclidian distance between participants within this vector space (Secundo et al., 2015). To test whether NAB1 and NAB2 may be closer to each other than expected by chance, the Euclidean distances between all subjects were calculated on reduced dimensions using principle components (PCs). In order to decide how many and which PCs to use for this calculation (Peres-Neto et al., 2005), we used bootstrapping (1000 iterations), which implied use of PCs 1 through 7.

QUANTIFICATION AND STATISTICAL ANALYSIS

Structural Imaging Analysis

For delineating and measuring the OB we developed software that automatically identifies the region of the OBs, and then allows the user to manually delineate OB boundaries across interpolated images, with all relevant slices displayed simultaneously on screen. This software was written by co-author LG, and is here made publicly available as Data S4. Using this in both the data we acquired, and in the HCP data, images were first independently reviewed by two experienced raters: lead-authors TW and TS, scientists with extensive experience in imaging and measuring the OB. Images were reviewed blind to participant identity and group-allocation, and raters demarcated OB borders for automated volume estimation (each rater completed this twice). The ensuing inter-rater correlation in volume estimation was $r = 0.93$, $p < 0.0001$. Moreover, the actual OB volumes fell squarely within previously published postmortem (Maresh et al., 2008) and MRI (Rombaux et al., 2009) measurements. Finally, all cases where a determination of no OB was made were submitted to a third blind review (presented interspersed with panels of other intact participant images) by co-author SS, an ENT-surgeon with extensive experience in MRI-based surgical decisions regarding these substrates.

For olfactory sulcus (OS) depth, we used ITK-SNAP version 3. First, in each slice where OBs were evident, a virtual tangent line was drawn from the inferior orbital gyrus to the gyrus recti. Next, a line was drawn from this tangent line to the deepest point of the OS. Finally, the slice with the maximal length of this line was taken to reflect OS depth.

For voxel-based morphometry we used FSL-VBM (https://fsl.fmrib.ox.ac.uk/fsl/fslwiki/FSLVBM) (Douaud et al., 2007). First, structural images were brain-extracted, gray matter-segmented, and registered to the MNI152 standard space using non-linear registration. The resulting images were averaged and flipped along the x axis to create a left-right symmetric, study-specific, gray matter template. Second, all native gray matter images were non-linearly registered to this study-specific template and "modulated" to correct for local expansion (or contraction) due to the non-linear component of the spatial transformation. The modulated gray matter images were then smoothed with an isotropic Gaussian kernel with a sigma of 3 mm. Finally, a voxelwise GLM was applied using permutation-based non-parametric testing, correcting for multiple comparisons across space.

MRI-based quantification of cortical thickness and subcortical volume were performed using Freesurfer version 6.0 software. The standard FreeSurfer preprocessing pipeline (recon-all) was applied to these images, in which a reconstruction of the cortical sheet was estimated using intensity and continuity information. Cortical thickness was determined as the closest distance from the gray matter/white matter boundary to the gray matter/cerebrospinal fluid boundary at each vertex. Surface area is estimated as the relative amount of expansion or compression at each vertex when registering each participant's surface to a common atlas. Subcortical volumes, and cortical thickness of regions associated with olfaction were extracted (Volumes: thalamus, pallidum, nucleus accumbens, hippocampus, amygdala. Thickness: parahippocampal gyrus, fusiform gyrus, insula, entorhinal cortex, medial and

lateral OFC, caudal and rostral middle-frontal gyrus, superior-frontal gyrus, rostral anterior-cingulate gyrus, frontal pole, and parsorbitails).

Diffusion MRI Analysis

All data was preprocessed by performing denoising (Veraart et al., 2016), removal of Gibbs ringing artifacts (Kellner et al., 2016), motion and eddy current distortion correction (Andersson et al., 2012), and bias field correction (Tustison et al., 2010). This was achieved using a combination of software packages: MRtrix3, FSL and ANTs. Next, we performed Single-Shell 3-Tissue Constrained Spherical Deconvolution (SS3T-CSD) on the preprocessed data, using 3-tissue response functions obtained from the data themselves using an unsupervised method (Dhollander and Connelly, 2016). This results in a white matter (WM)-like fiber orientation distribution (FOD), and gray matter (GM)-like and cerebrospinal fluid (CSF)-like compartments in each voxel (Dhollander et al., 2017). The WM-like FOD represents anisotropic, and hindered or restricted, diffusion as found in, e.g., tightly packed bundles of axons (but also, for instance, in muscle tissue). The presence of GM-like and CSF-like compartments in the model filters out signals from other tissues (Dhollander et al., 2017). Finally, the FOD images were mapped to a common template space (at a voxel size of $1.5 \times 1.5 \times 1.5$ mm^3) using an FOD informed registration approach (Raffelt et al., 2011). The resulting FOD images were overlaid on an FOD-based directionally encoded color (DEC) map for visualization.

Functional MRI Analysis

We used FSL (FMRIB's Software Library) FEAT (FMRI Expert Analysis Tool) Version 6.00 (Woolrich et al., 2001), and MATLAB R2018a (MathWorks, Inc.)

Preprocessing

Preprocessing steps included motion correction using MCFLIRT, removal of non-brain regions using BET, high-pass temporal filtering (cutoff period = 125 s) to remove signal drift, and spatial smoothing using a Gaussian kernel of 6 mm full-width at half-maximum. This was followed by correction of time series autocorrelation, resampling of functional data to $1 \times 1 \times 1$ mm^3 isotropic voxels, and registration to MNI template space using nonlinear registration (warp resolution = 10 mm).

To Generate Statistical Parametric Maps of Odorant-Induced Activation

For each participant, a first-level general linear model included one regressor of interest, and its temporal derivative. The start time and duration of each inhale during odor presentation was modeled and convolved with a canonical (double gamma) hemodynamic response function. This model also included a regressor of no interest for each volume, with > 0.9 mm framewise displacement. Voxel-wise beta values were estimated for odorant events in contrast to clean air (the ISI). One participant (Control #15 in Table S1) was excluded due to atypical hemodynamic response. The two functional runs of each subject were submitted to a fixed effects analysis. Between-group and within-control-group analyses were completed by using non-parametric permutation analysis (randomize, FSL). Correction for multiple comparisons was maintained by FSL's threshold free cluster enhancement (TFCE). In all functional MRI analyses we used the term whole-brain for all the voxels in the FOV.

To Extract Piriform Time-Course

We used previously published statistical localization for odor versus baseline contrasts (Seubert et al., 2013): the right and left piriform were defined by the peak coordinates [22,2,-12], [-22,0,-14], with a 4 mm sphere. For secondary olfactory: peak coordinates of right insula [36,24,-2] and the right OFC [28,34,-12] were defined with a 6 mm sphere. The Featquery tool was used for parametric estimation extraction (the mean % signal change) across all voxel in each ROI for each participant. The averaged % signal change graph was created by extraction of the average time course of each voxel (fslmeants), normalization (dividing by the mean time course), followed by extraction and averaging of all epochs.

To Estimate Functional Connectivity

we used psychophysiological interaction (PPI) analysis (Friston et al., 1997) to measure changes in functional connectivity modulated by odor presentation. We conducted whole-brain PPI tests, reflecting greater correlation with seed ROI time series (physiological regressor) for odor presentation (odors > clean-air) (psychological regressor). Separate analyses were conducted for the three seed ROIs: right piriform, left piriform and right insula. We used FLAME1 (FMRIB's Local Analysis of Mixed Effects) for group analysis, and cluster-size correction $z > 2.58$ ($p < 0.005$).

To Estimate Valence-Related Activity

We repeated the analysis using the participant pleasantness rating as a parametric modulation value (weightings for the most unpleasant: −0.75, unpleasant: −0.25, pleasant: 0.25, and the most pleasant: 0.75) (Figure S8). This model also included a regressor of no interest for each volume, with > 0.9 mm framewise displacement (Siegel et al., 2014). We used FLAME1 for group analysis, and cluster-size correction $z > 2.3$ ($p < 0.01$).

Behavioral Statistics

Because we often compare one participant to a group, we calculated all t values using a two-tailed Crawford & Howell's modified t test (where $t = \frac{x - \bar{x}}{s(\bar{x}) * \mathrm{sqrt}((n+1)/n}$, x: value of the case study; x: group control mean; s(x): group control standard deviation; n: number of participants in the group), which was developed specifically for such instances (Crawford and Garthwaite, 2005). This method treats the control sample statistics as statistics rather than as parameters. Monte Carlo simulations confirm that this test controls for Type I error rate regardless of the size of the control sample (Crawford and Garthwaite, 2005). In all these cases, we further estimated effect size using Z-CC, a method developed for comparisons between a group and an individual (Crawford et al., 2010). This index is the direct analog of Cohen's d when comparing a single-case's score to a control sample. It expresses the difference between a single-case's score (x) and the controls' sample mean (x) in standardized units by dividing that difference by the standard deviation of the control group. Z-CC = $(x - (\bar{x}) / s(\bar{x}))$. The subscript CC representing "case-controls." As in Z scale, score of -0.674 representing a score only slightly below the population mean, -1.282 (10%), -1.960 (2.5%), and -2.326 representing a very low score; only 1% of the control population would obtain a lower score. This index is an estimate of the average difference, measured in standard deviation units so as to be scale independent, between a case's score and the score of a randomly chosen member of the control population. Like Cohen's d, Z-CC is insensitive to the size of the control sample which is a required characteristic for an index of effect size.

In all other cases of comparing between groups (rather than group versus individual) we used either standard t tests following by Cohen's d' estimations of effect size, or non-parametric statistics in cases of non-normally distributed data. Throughout the manuscript, results are reported as mean ± standard deviation, and all reported p values reflect two-tailed tests.

DATA AND CODE AVAILABILITY

This study did not generate new unique reagents.

Original/source data for all imaging experiments is available at OpenNeuro, https://doi.org/10.18112/openneuro.ds002185.v1.0.0.

Original/source data for all behavioral experiments is available at https://www.weizmann.ac.il/neurobiology/worg/materials.html.